optica

Quantum fast hitting on glued trees mapped on a photonic chip: supplementary material

ZI-YU SHI[1,2], HAO TANG[1,2], ZHEN FENG[1,2], YAO WANG[1,3], ZHAN-MING LI[1,2], JUN GAO[1,3], YI-JUN CHANG[1,2], TIAN-YU WANG[1,2], JIAN-PENG DOU[1,2], ZHE-YONG ZHANG[1,2], ZHI-QIANG JIAO[1,2], WEN-HAO ZHOU[1,2], AND XIAN-MIN JIN[1,3,*]

[1]*Center for Integrated Quantum Information Technologies (IQIT), School of Physics and Astronomy and State Key Laboratory of Advanced Optical Communication Systems and Networks, Shanghai Jiao Tong University, Shanghai 200240, China*

[2]*CAS Center for Excellence and Synergetic Innovation Center in Quantum Information and Quantum Physics, University of Science and Technology of China, Hefei, Anhui 230026, China*

[3]*Shenzhen Institute for Quantum Science and Engineering and Department of Physics, Southern University of Science and Technology, Shenzhen 518055, China*

[*]*Corresponding author: xianmin.jin@sjtu.edu.cn*

Published 27 May 2020

This document provides supplementary information to "Quantum fast hitting on glued trees mapped on a photonic chip," https://doi.org/10.1364/OPTICA.388451 giving a detailed explanation about the mapping of the glued trees to a 1D chain, the fabrication of waveguides, the single-photon imaging process, the data-processing methods and the measurement of anti-correlation parameter.

SUPPLEMENTARY NOTE 1 - SIMPLIFICATION PROCESS OF THE RANDOM GLUED TREES TO A 1D CHAIN

We will first give the general derivation process [S1] of QW; then, we will give a simple example to make the general derivation easily understood; finally, we will analyze the simplification process of CRW.

Consider the Hilbert space of the 1D chain spanned by $|\,\mathrm{col}\,j\rangle$, which can be represented as the uniform superposition over the nodes in column j, i.e.,

$$|\,\mathrm{col}\,j\rangle = \frac{1}{\sqrt{N_j}} \sum_{a\in \mathrm{column}\,j} |a\rangle \tag{S1}$$

where $|a\rangle$ represents the state of a node on the glued trees, and N_j is the number of nodes in column j.

$$N_j = \begin{cases} B^j & 0 \le j \le n \\ B^{2n+1-j} & n+1 \le j \le 2n+1 \end{cases} \tag{S2}$$

If the adjacency matrix of the random glued trees is represented by A, in which, if two nodes i and j are connected, $A_{i,j} = 1$, otherwise, $A_{i,j} = 0$, then we have the following derivation process. We assume the hopping rate γ of random glued trees is 1, hence the Hamiltonian $H = A$. For any $0 < j < n$, we have

$$\begin{aligned} A|\,\mathrm{col}\,j\rangle &= \frac{1}{\sqrt{N_j}} \sum_{a\in \mathrm{column}\,j} A|a\rangle \\ &= \frac{1}{\sqrt{N_j}} \left(B \sum_{a\in \mathrm{column}\,j-1} |a\rangle + \sum_{a\in \mathrm{column}\,j+1} |a\rangle \right) \\ &= \frac{1}{\sqrt{N_j}} \left(B\sqrt{N_{j-1}}|\,\mathrm{col}\,j-1\rangle + \sqrt{N_{j+1}}|\,\mathrm{col}\,j+1\rangle \right) \\ &= \sqrt{B}(|\,\mathrm{col}\,j-1\rangle + |\,\mathrm{col}\,j+1\rangle). \end{aligned} \tag{S3}$$

In a similar way, for any $n+1 < j < 2n+1$, we have

$$\begin{aligned} A|\,\mathrm{col}\,j\rangle &= \frac{1}{\sqrt{N_j}} \left(\sum_{a\in \mathrm{column}\,j-1} |a\rangle + B \sum_{a\in \mathrm{column}\,j+1} |a\rangle \right) \\ &= \frac{1}{\sqrt{N_j}} \left(\sqrt{N_{j-1}}|\,\mathrm{col}\,j-1\rangle + B\sqrt{N_{j+1}}|\,\mathrm{col}\,j+1\rangle \right) \\ &= \sqrt{B}(|\,\mathrm{col}\,j-1\rangle + |\,\mathrm{col}\,j+1\rangle). \end{aligned} \tag{S4}$$

We can see that the hopping rates on the chain which correspond to the left tree and the right tree are uniform, and are $\sqrt{B}$ times of that on the original graph.

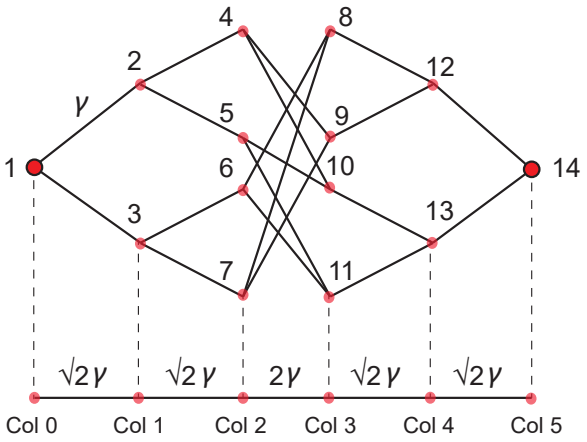

Fig. S1. Schematic diagram of random glued trees with B=2, n=2.

However, when comes to the mapping of the random-glued part of the glued trees, the results are different. The random-glued part has to satisfy the condition that each node in column n should be connected to B different nodes in column $n+1$, and vice versa. Then, if $j = n$, we have

$$\begin{aligned} A|\,\mathrm{col}\,n\rangle &= \frac{1}{\sqrt{N_n}}\left(B\sum_{a\in\mathrm{column}\,n-1}|a\rangle + B\sum_{a\in\mathrm{column}\,n+1}|a\rangle\right) \\ &= \frac{1}{\sqrt{N_n}}\left(B\sqrt{N_{n-1}}|\,\mathrm{col}\,n-1\rangle + B\sqrt{N_{n+1}}|\,\mathrm{col}\,n+1\rangle\right) \\ &= \sqrt{B}|\,\mathrm{col}\,n-1\rangle + B|\,\mathrm{col}\,n+1\rangle. \end{aligned} \tag{S5}$$

Similarly,

$$\begin{aligned} A|\,\mathrm{col}\,n+1\rangle &= \frac{1}{\sqrt{N_{n+1}}}\left(B\sum_{a\in\mathrm{column}\,n}|a\rangle + B\sum_{a\in\mathrm{column}\,n+2}|a\rangle\right) \\ &= \frac{1}{\sqrt{N_{n+1}}}\left(B\sqrt{N_n}|\,\mathrm{col}\,n\rangle + B\sqrt{N_{n+2}}|\,\mathrm{col}\,n+2\rangle\right) \\ &= B|\,\mathrm{col}\,n\rangle + \sqrt{B}|\,\mathrm{col}\,n+2\rangle. \end{aligned} \tag{S6}$$

We can see that the hopping rate on the chain corresponding to the random-glued part is B times of the hopping rate on the glued trees, different from the rest of the hopping rates. It is obvious that what exactly the random-glued part is does not affect the geometry of the 1D chain. Next, we will use a simple example to illustrate the above derivation process.

If $|\,\mathrm{col}\,0\rangle, |\,\mathrm{col}\,1\rangle, |\,\mathrm{col}\,2\rangle, |\,\mathrm{col}\,3\rangle$ can be represented as

$$|\,\mathrm{col}\,0\rangle = |1\rangle, \tag{S7}$$

$$|\,\mathrm{col}\,1\rangle = \frac{1}{\sqrt{2}}(|2\rangle + |3\rangle), \tag{S8}$$

$$|\,\mathrm{col}\,2\rangle = \frac{1}{\sqrt{4}}(|4\rangle + |5\rangle + |6\rangle + |7\rangle), \tag{S9}$$

$$|\,\mathrm{col}\,3\rangle = \frac{1}{\sqrt{4}}(|8\rangle + |9\rangle + |10\rangle + |11\rangle), \tag{S10}$$

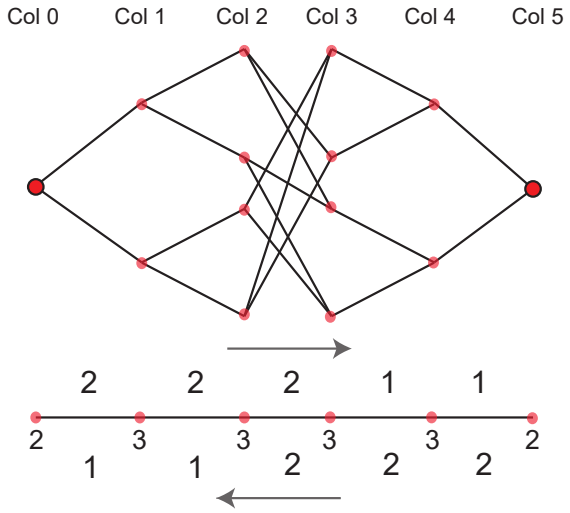

Fig. S2. Schematic diagram of CRW's 1D equivalence with B=2, n=2. The numbers above the 1D chain are the hopping rates in the forward direction which are determined by the number of edges connected to the right side node, and the numbers below the 1D chain are the hopping rates in the backward direction which are determined by the number of edges connected to the left side node. The number under each node on the 1D chain presents the outdegree of this node.

then,

$$\begin{aligned} A|\,\mathrm{col}\,1\rangle &= \frac{1}{\sqrt{2}}A(|2\rangle + |3\rangle) \\ &= \frac{1}{\sqrt{2}}(|1\rangle + |4\rangle + |5\rangle + |1\rangle + |6\rangle + |7\rangle) \\ &= \frac{1}{\sqrt{2}}(2|\,\mathrm{col}\,0\rangle + \sqrt{4}|\,\mathrm{col}\,2\rangle) \\ &= \sqrt{2}(|\,\mathrm{col}\,0\rangle + |\,\mathrm{col}\,2\rangle). \end{aligned} \tag{S11}$$

$$\begin{aligned} A|\,\mathrm{col}\,2\rangle &= \frac{1}{\sqrt{4}}A(|4\rangle + |5\rangle + |6\rangle + |7\rangle) \\ &= \frac{1}{\sqrt{4}}(|2\rangle + |9\rangle + |10\rangle + |2\rangle + |10\rangle + |11\rangle \\ &+ |3\rangle + |8\rangle + |11\rangle + |3\rangle + |8\rangle + |9\rangle) \\ &= \frac{1}{\sqrt{4}}(2\sqrt{2}|\,\mathrm{col}\,1\rangle + 2\sqrt{4}|\,\mathrm{col}\,3\rangle) \\ &= \sqrt{2}|\,\mathrm{col}\,1\rangle + 2|\,\mathrm{col}\,3\rangle. \end{aligned} \tag{S12}$$

The hopping rates between $|\,\mathrm{col}\,0\rangle$ and $|\,\mathrm{col}\,1\rangle$, $|\,\mathrm{col}\,1\rangle$ and $|\,\mathrm{col}\,2\rangle$, $|\,\mathrm{col}\,2\rangle$ and $|\,\mathrm{col}\,3\rangle$ on the chain are $\sqrt{2}$, $\sqrt{2}$, 2 respectively. It is obvious that, as long as the random-glued part satisfies that each node in column 2 is connected to 2 different nodes in column 3, and vice versa for column 3, the specific connection way does not affect the structure of the 1D chain. The hopping rates between the remaining nodes on the chain can be derived in a similar way.

Obviously, it is the superposition property of QW, which is embodied by equation (S1), that makes this simplification process possible. However, when comes to the analysis of CRW, the methods and results are totally different. We'll see that CRW can also be simplified to a 1D model and the hitting efficiency is

consistent with that of the original two-dimensional structure which exponentially decays with the tree depth.

For CRW, its probability vector can be obtained by

$$\mathbf{p}(t) = \mathrm{e}^{-Mt} \cdot \mathbf{p}(0), \tag{S13}$$

with generator matrix M satisfies

$$M_{ij} = \begin{cases} -\gamma A_{ij}, & i \neq j \\ \gamma d(j), & i = j \end{cases} \tag{S14}$$

in which, γ is the hopping rate between two adjacent nodes; $d(j)$ is the outdegree of the jth node, i.e. the number of edges that the jth node connects to the other nodes [S2].

For the classical case, on the one hand, classical particle does not have superposition property, hence Equation (S1) cannot stand. On the other hand, we can clearly see that in the left part of the glued tree, each node is connected to B branches forward and 1 branch backward, so the forward probability from column j to $j+1$ is B times of the backward probability from column $j+1$ to j, and vice versa for the columns in the right part of the glued trees. Hence, the analysis of CRW's probability distribution on the random glued trees can also be reduced to a 1D chain as shown in Fig.S2 [S3][S4].

For CRW, when evolving time is long enough, its probability distribution will be uniform and stationary, and the hitting probability at each node is the inverse of the number of nodes on the glued trees. The number of nodes on the glued trees N is in an exponential relation with n. Utilizing the M matrix of the 1D chain for calculation, we can get the probability of each node on the chain reaches a stationary value of $1/N$, which is consistent with the theoretical result for classical hitting in the 2D structure. Different from QW, the jth node on CRW's 1D chain just represents one node in the jth column of the 2D graph rather than the whole column, and the sum of the probability of such classical 1D chain does not equal to 1. The simplification process of the CRW on random glued trees may be useful for the theoretical calculation of the CRW on the other symmetrical graphs[S3].

SUPPLEMENTARY NOTE 2 - THE SENSITIVITY ANALYSIS OF THE EXPERIMENTAL RESULTS WITH RESPECT TO THE COUPLING COEFFICIENTS

The main reason that causes the experimental results different from the theoretical values is the experimental coupling coefficients differing from the theoretical hopping rates. It will lead to an inaccurate implementation of the hopping rate γ and branching rate B. The inaccurate realization of B will alter the optimal hitting efficiency, while the inaccurate realization of γ will alter the optimal evolving length. We will use the theoretical simulation of glued trees with $n = 16$ and $B = 5$ as an example to quantitatively illustrate the effects of the deviation of C to the results.

In Fig.S3 (a), the branching rate B is kept as 5. We can see that when decreasing γ from $0.1163mm^{-1}$ to $0.0983mm^{-1}$ (the C corresponding to $\sqrt{B}\gamma$ decreasing from $0.26mm^{-1}$ to $0.22mm^{-1}$ correspondingly), the optimal evolving length increases by 13mm (15.7%) while the optimal hitting efficiency doesn't change. In Fig.S3 (b), keep γ as $0.1163mm^{-1}$, and increase B from 5 to 6 (the C corresponding to $\sqrt{B}\gamma$ increasing from $0.26mm^{-1}$ to $0.285mm^{-1}$ correspondingly), then we can see the optimal hitting efficiency decreases from 0.268 to 0.234, decreasing about 12.7%. It is obvious that the experimental results are highly sensitive to the precision of the coupling coefficients. What's more, on the one hand, there exists errors in the measurements of the coupling coefficient. On the other hand, the C is in an exponential relation with respect to d, and a slight change of environment or direct-writing laser will change the specific function of C. Therefore, the successful implementation of glued trees' 1D equivalence in experiment is really challenging.

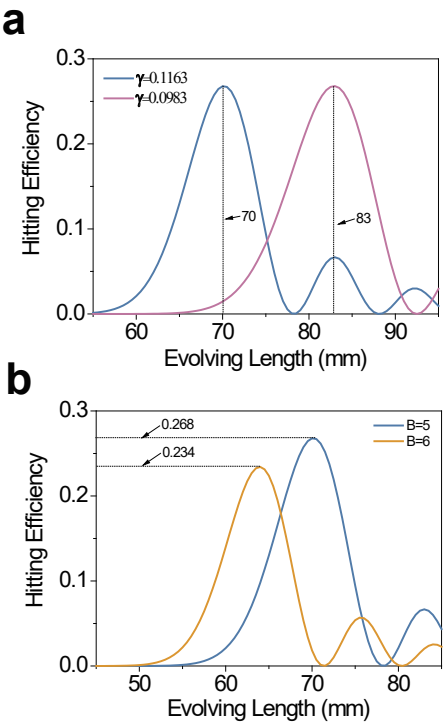

Fig. S3. The influence of the errors in γ or B on the results. **a,** $B = 5$, γ is decreased from $0.1163mm^{-1}$ to $0.0983mm^{-1}$, the C corresponding to $\sqrt{B}\gamma$ decreasing from $0.26mm^{-1}$ to $0.22mm^{-1}$ correspondingly. The optimal evolving length increases by 13mm (15.7%) while the optimal hitting efficiency does not change. **b,** $\gamma = 0.1163mm^{-1}$, B is increased from 5 to 6, the C corresponding to $\sqrt{B}\gamma$ increasing from $0.26mm^{-1}$ to $0.285mm^{-1}$ correspondingly. The optimal hitting efficiency decreases from 0.268 to 0.234, decreasing about 12.7%.

To improve the repeatability, one should keep the C of the experimental chip consistent with the C-measurement chip as much as one can. The parameters of the laser (e.g., the shape, the power), and the condition of the environment (e.g., the temperature, the humidity) all should be kept the same. The interval time between the fabrication of the C-measurement chip and the experimental chip should be reduced as short as possible to avoid parameters changing with time. The fabrication time of the experimental chips had better not exceed 3 hours. Through these efforts, the repeatability of this work can be much ensured.

SUPPLEMENTARY NOTE 3 - FABRICATION OF THE WAVEGUIDE ARRAYS

In the femtosecond laser direct writing process, the writing laser with a wavelength of 513nm is up-converted from a femtosecond laser with a wavelength of 1026nm, a pulse duration of 290 fs, and a repetition rate of 1 MHz, and is firstly sent through a spa-

tial light modulation (SLM) and then focused on a borosilicate chip substrate through a $50\times$ objective lens. The waveguide is written at a depth of $380um$ with a velocity of $10mm/s$. To insure the uniformity of the waveguide arrays, power compensation are also used. The optimal range of d is about $10\mu m$-$15\mu m$, and corresponding coupling coefficient ranges from $0.15mm^{-1}$ to $0.6mm^{-1}$. The coupling coefficients used in this work range from $0.22mm^{-1}$ to $0.6mm^{-1}$.

As for the determination of the waveguide spacing d and measurement of the coupling coefficient C, the method can be described as follows. First, we write waveguide pairs of different waveguide spacings and measure the output intensity distribution at different evolving lengths, hence we can obtain the C at different d [S5], e.g. 10, 12, 14, 16, 18 μm. Next, we use exponential function to fit the obtained $C-d$ data, so that we can get the specific function of coupling coefficient and waveguide spacing, from which we can obtain the corresponding d if the C is given. Then, considering the experimental feasibility, we choose suitable coupling coefficient to calculate corresponding optimal evolving length. Finally, for graphs of each size, we fabricate waveguide arrays at different lengths with waveguide spacings consistent with the coupling coefficients used in theoretical calculation.

The specific values of d for the case of branching rate $B=3$ are given as an example (Table S1). For $B=3$, the C that corresponds to the hopping rate $\sqrt{B}\gamma$ of the 1D structure is $0.2843mm^{-1}$ and the C that corresponds to the hopping rate $B\gamma$ of the 1D structure is $0.4924mm^{-1}$. The values of d for different layer depth n shown in Table S1 is slightly different. It's because the precise relationship between C and d may slightly vary when the condition of the femtosecond laser and the environment changes. Therefore, every time before we decide to fabricate an experimental chip, we will calibrate the function of C with respect to d again, which always follows an exponential decay.

Table S1. Waveguide spacing d at different n for the case of B=3. The hopping rate $\sqrt{B}\gamma$ or $B\gamma$ refer to the hopping rate of the 1D structure.

n	d (μm) for $\sqrt{B}\gamma$	d (μm) for $B\gamma$
2	13	10.8
4	13	10.8
6	13	10.8
8	12.8	10.4
10	13.6	10.6
12	13.6	10.6
14	13.6	10.6
16	13.6	10.6

SUPPLEMENTARY NOTE 4 - SINGLE-PHOTON IMAGING OF SPATIAL PHOTON NUMBER DISTRIBUTIONS

To carry out the experiment in the quantum regime, we use heralded single photons as the photon source (Fig. S8). The 810nm photon pairs are generated via a type-II spontaneous parametric down conversion (SPDC) process, pumped by an ultraviolet laser with a wavelength of 405nm in a PPKTP crystal. The generated photon pairs are sent through a long-pass filter and then separated into horizontal and vertical component by utilizing a polarized beam splitter(PBS). The vertically-polarized photons are injected into the waveguide arrays, playing the role of quantum walkers, while the horizontally-polarized photons are used to give the ICCD camera a photographing command via a single-photon detector (APD). The photographing commands triggered by the horizontally-polarized photons are used to avoid the impact of thermal light statistics and can considerably suppress the noise level.

SUPPLEMENTARY NOTE 5 - CALCULATION OF THE HITTING EFFICIENCY

By photographing the spatial photon number distributions of single photons via an ICCD, we obtain the picture as well as a corresponding ASCII file which records the photon intensity of each pixel. We first find the center pixel coordinate for each waveguide shown in the picture, and then measure the radius in terms of pixel counts for the light spot in each waveguide. By summing up the intensity value within the radius and normalizing them, we get the probabilities of photons distributed at each waveguide.

SUPPLEMENTARY NOTE 6 - SPATIAL PHOTON NUMBER DISTRIBUTIONS AND SCALINGS OF OPTIMAL EVOLVING LENGTH

The experimental results for trees with $B=2, 3, 4, 5$ are presented in Fig. S4-S7 respectively. Each figure shows spatial photon number distributions of optimal hitting efficiencies and scalings of the corresponding optimal evolving lengths with n ranging from 2 to 16. Optimal evolving length refers to the evolving length at which optimal hitting efficiency occurs. Note that hopping rate γ between two adjacent nodes on random glued trees will influence the optimal evolving length, hence we set the same hopping rate for all the four scaling plots shown in Fig. S4-S7. The linear scaling is clearly suggested by the theoretical calculation and is well agreed by the experimental results. For samples at the same B, though optimal hitting efficiency decreases slightly with the increasing number of waveguides as n increases, most of the photons would gather at the exit waveguide when optimal hitting efficiency occurs. Comparing spatial photon number distributions of the same n in different Bs, there is an overall drop of the light intensity at the exit waveguide from $B=2$ to $B=5$. This leads to the slight decrease of optimal hitting efficiency as B increases, and is consistent with theoretical studies [S6].

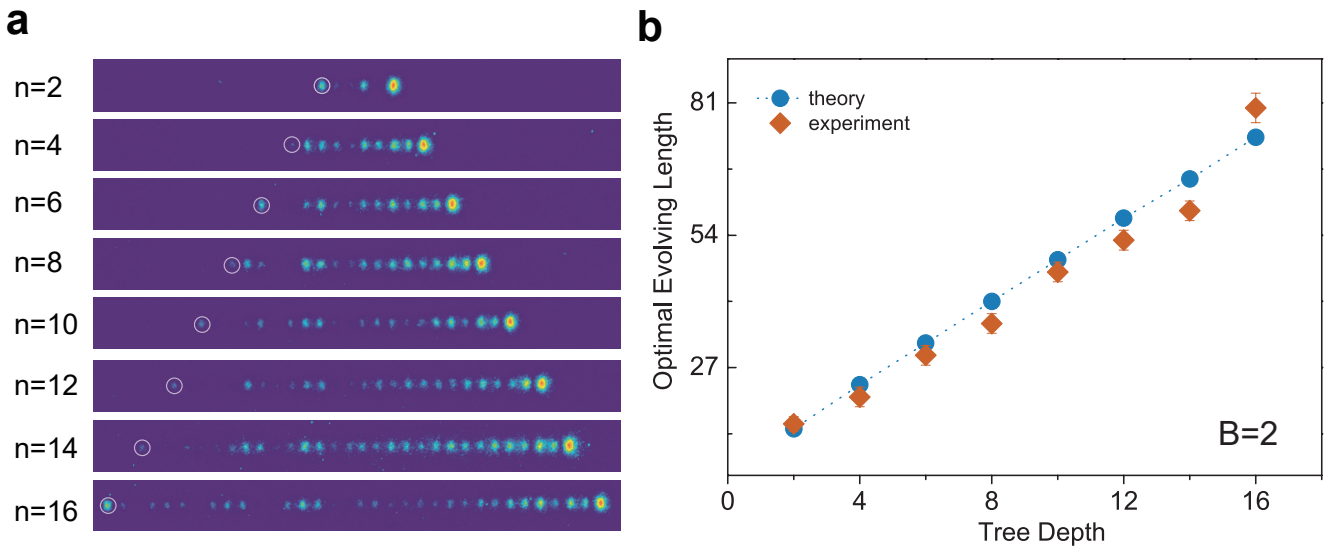

Fig. S4. Spatial photon number distributions and scalings of optimal evolving lengths for samples at $B = 2$. a, Spatial photon number distributions of optimal hitting efficiency from 2-layer to 16-layer at $B = 2$. The injecting waveguide is marked by a white circle. **b,** Variation of optimal evolving lengths with n ranging from 2 to 16 in theory and experiment respectively. Error bars for the experimental optimal evolving lengths are the intervals of evolving length values between two adjacent samples at the same n and B used in experiments. Since evolving length values are discrete in experiment, the optimal evolving length may lie between two adjacent waveguide length values. The error bar descriptions also apply to Fig. S5, S6 and S7.

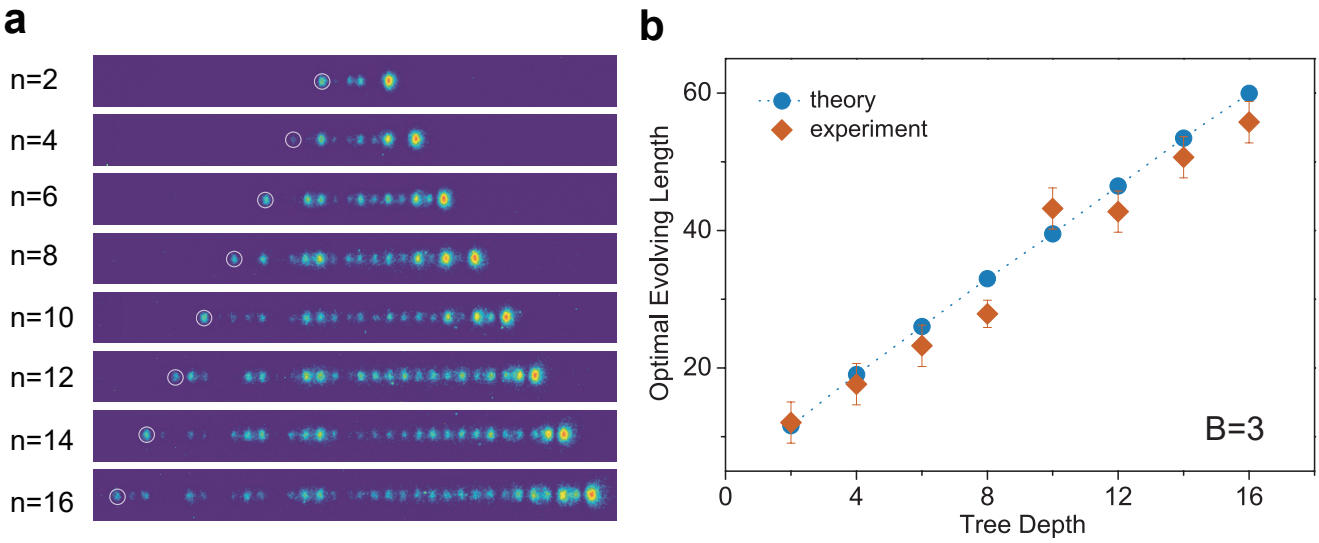

Fig. S5. Spatial photon number distributions and scalings of optimal evolving lengths for samples at $B = 3$. a, Spatial photon number distributions of optimal hitting efficiency from 2-layer to 16-layer at $B = 3$. The injecting waveguide is marked by a white circle. **b,** Variation of optimal evolving lengths with n ranging from 2 to 16 in theory and experiment respectively.

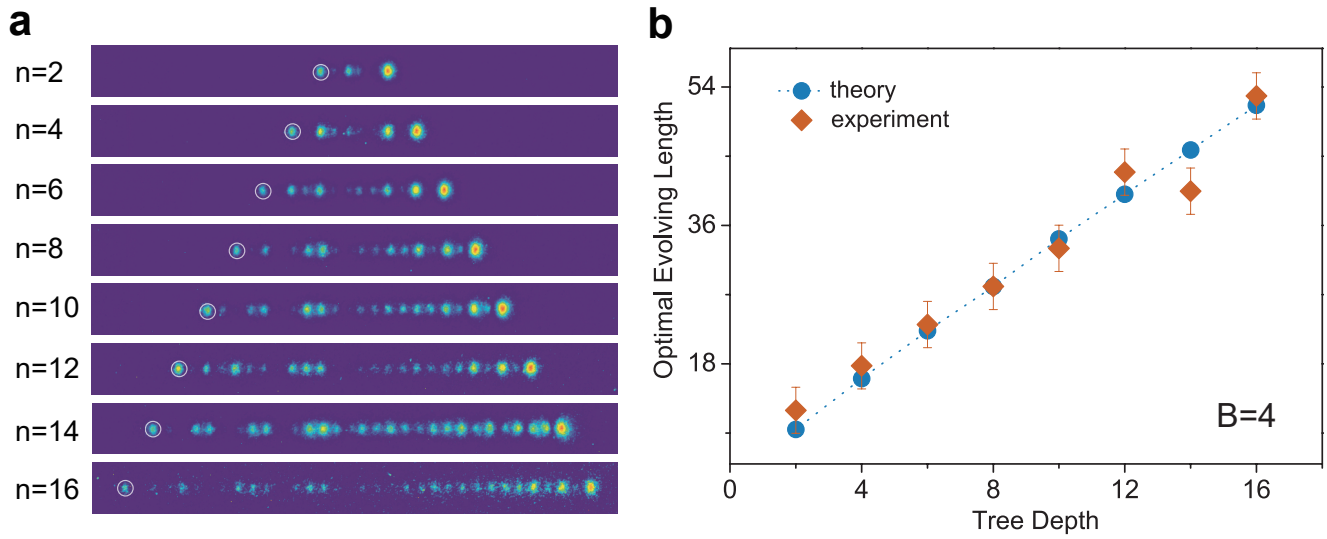

Fig. S6. Spatial photon number distributions and scalings of optimal evolving length for samples at $B = 4$. **a,** Spatial photon number distributions of optimal hitting efficiency from 2-layer to 16-layer at at $B = 4$. The injecting waveguide is marked by a white circle. **b,** Variation of optimal evolving lengths with n ranging from 2 to 16 in theory and experiment respectively.

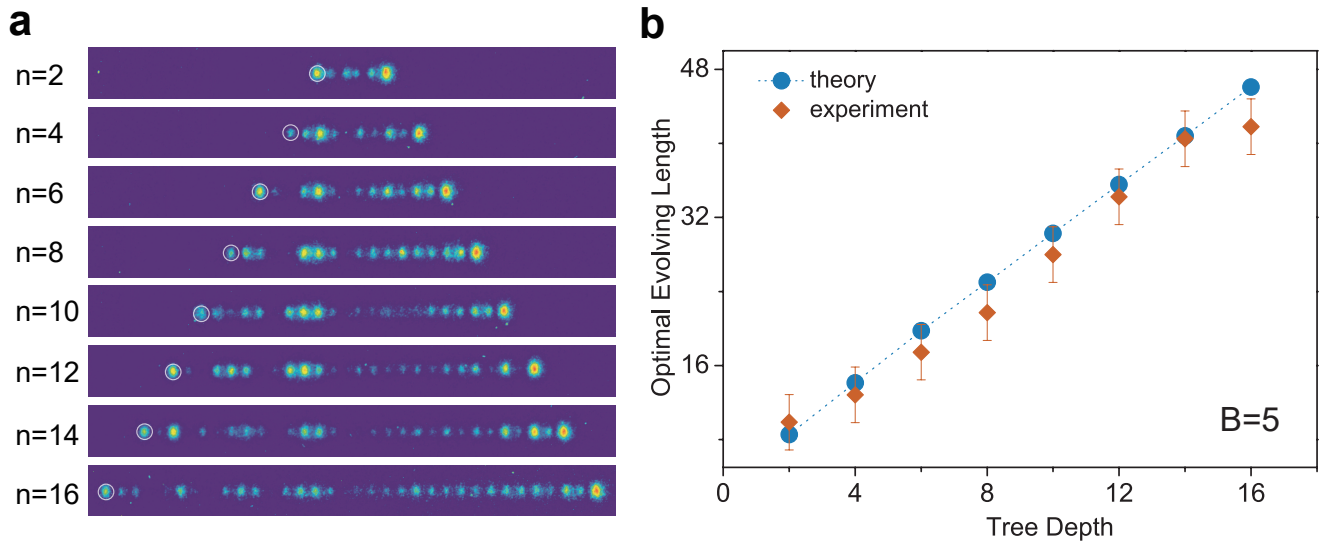

Fig. S7. Spatial photon number distributions and scalings of optimal evolving length for samples at $B = 5$. **a,** Spatial photon number distributions of optimal hitting efficiency from 2-layer to 16-layer at $B = 5$. The injecting waveguide is marked by a white circle. **b,** Variation of optimal evolving lengths with n ranging from 2 to 16 in theory and experiment respectively.

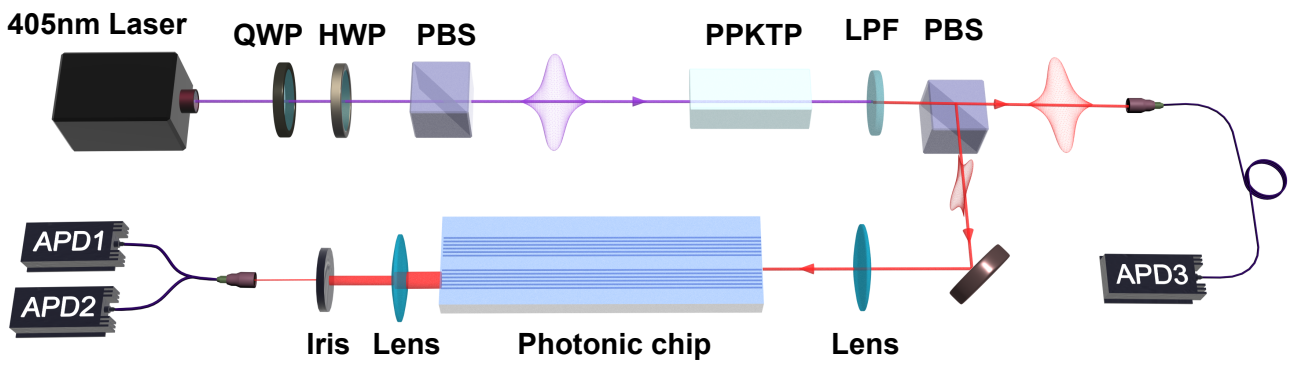

Fig. S8. Setup of measuring α. A 405nm laser pumping a PPKTP crystal can generate 810nm correlated photon pairs via the type-II SPDC process. A long pass filter (LPF) is inserted to block the pump laser. Then the photon pairs pass through a PBS and are separated into vertically-polarized photons and horizontally-polarized photons. The horizontally-polarized photons play the role of trigger signal and are detected by an avalanched photodiode (APD3); the vertically-polarized photons are injected into the photonic chip. Then, an iris is used to filter out the photons coming from the exit waveguide. Finally, the out-coming photons are coupled into a balanced fiber beam splitter and detected by two separate APDs (APD1 and APD2). A photon coincidence counter module (not shown in the picture) is utilized to record the coincidence events. This setup can be switched into the single-photon imaging of spatial photon number distribution by replacing APD1, APD2 and the fiber beam splitter with an ICCD camera. QWP, quarter-wave plate; HWP, half-wave plate; PBS, polarized beam splitter; PPKTP, periodically poled KTP crystal; LPF, long-pass filter; APD, avalanched photodiode.

SUPPLEMENTARY NOTE 7 - MEASUREMENTS OF SECOND-ORDER ANTI-CORRELATION PARAMETER α

The second-order anti-correlation parameter α, which tends to be 0 for ideal single photon and 1 for classical coherent light, can be described as [S7]

$$\alpha = \frac{N_3 N_{123}}{N_{13} N_{23}}, \tag{S15}$$

where N_3 represents the number of trigger signals; $N_{23}(N_{13})$, N_{123} represent the number of two- and three-fold coincidence detection events.

As shown in Fig. S8, one arm of the single photon pairs that generated in the SPDC single photon source is used as the trigger signal, and another is injected into the waveguide arrays. The number of trigger signal can be detected by an avalanched photodiode (APD3), through which we can obtain N_3. As for the photons being injected into the waveguide arrays, when they have exited the photonic chip, those coming from the exit waveguide are filtered out by an iris inserted after the chip, then the out-coming photons are coupled into a balanced fiber beam splitter and detected by two separate APDs (APD1 and APD2), hence we can obtain the rest of the coincidence detection events. A photon coincidence counter module (not shown in the picture) is utilized to record the coincidence events.

SUPPLEMENTARY REFERENCE

[S1] Retrieved from: https://www.math.uwaterloo.ca/~amchilds/teaching/w08/l13.pdf
[S2] P. E. Falloon, J. Rodriguez and J. B. Wang, "QSWalk: a Mathematica package for quantum stochastic walks on arbitrary graphs," Comput. Phys. Commun. **217**, 162-170 (2017)
[S3] A. M. Childs, E. Farhi, and S. Gutmann, "An example of the difference between quantum and classical random walks," Quantum Inf. Process. **1**, 35-43 (2002)
[S4] S. R. Jackson, T. J. Khoo and F. W. Strauch, "Quantum walks on trees with disorder: decay, diffusion, and localization," Phys. Rev. A **86**, 2 (2012)
[S5] A. Szameit, F. Dreisow, T. Pertsch, S. Nolte, and A. Tünnermann, "Control of directional evanescent coupling in fs laser written waveguides," Opt. Express **15**, 1579-1587 (2007)
[S6] I. Carneiro, M. Loo, X. Xu, M. Girerd, V. Kendon, and P. L. Knight, "Entanglement in coined quantum walks on regular graphs," New J. Phys. **7**, 156 (2005)
[S7] J. B. Spring, P. S. Salter, B. J. Metcalf, P. C. Humphreys, M. Moore, N. Thomas-Peter, M. Barbieri, X.-M. Jin, N. K. Langford,W. S. Kolthammer *et al.*, "On-chip low loss heralded source of pure single photons," Opt. Express **21**, 13522-13532 (2013)